Multiphoton ghost imaging with classical light

I. N. Agafonov, M. V. Chekhova, A. N. Penin
Department of Physics,
M.V.Lomonosov Moscow State University,
Leninskie Gory, 119992 Moscow, Russia

One of the possible types of n-th order ghost imaging is experimentally performed using multi-photon (higher-order) intensity correlations of pseudothermal light. It is shown that although increasing the order of intensity correlations leads to the growth of ghost imaging visibility, it at the same time reduces the signal-to-noise ratio. Therefore, ghost imaging with thermal light is optimal in the second order in the intensity.

PACS numbers: 42.50.Dv, 03.67.Hk, 42.62.Eh

INTRODUCTION

The technique of ghost imaging (GI), first demonstrated in 1995 [1], still attracts much interest in connection with remote sensing [2], lenseless imaging [3], and fundamental problems, such as the boundary between quantum and classical physics (see, for instance, [4]). The idea of ghost imaging is based on the correlations existing between the intensities of two beams, which will be further called the signal one and the reference one. The object to be imaged (a mask) is placed into the signal beam, and the photons transmitted through it are registered by a "bucket" detector, which collects all signal radiation and hence does not resolve the shape of the mask. The detector in the reference beam, on the contrary, is spatially resolving, but there is no mask in the reference beam. The coincidences, or photocurrent correlations, of signal and reference detectors are registered as a function of the reference detector position. When the reference detector registers photons whose correlated signal counterparts pass through the mask, there is an increase in the coincidence counting rate (photocurrent correlation function). Thus, by scanning the reference detector one restores the image of the mask in the signal beam.

Although ghost imaging was at first supposed to require two-photon light generated via spontaneous parametric down-conversion (SPDC), it was later demonstrated with classical light [17], in particular, pseudothermal light obtained by passing a coherent beam through a rotating ground-glass disk [6, 7, 8] and true thermal light [9]. In a large number of works, both near-field and far-field ghost imaging with pseudo-thermal light was performed, as well as ghost imaging of a purely phase object [10] or a reflecting object [2]. It seemed that the only advantage of using nonclassical light for ghost imaging was a higher visibility than in the case of thermal light. However, in several works it was proposed to increase the visibility of ghost imaging with classical light by increasing the value of normalized correlation function. In Ref. [11], it was performed by introducing a threshold for the bucket detector output and hence choosing only peaks of the intensity fluctuations. In Ref. [12], it was suggested to use the fact that the normalized intensity correlation function (CF) of the n-th order for thermal light grows as $n!$ and thus to increase the visibility of ghost imaging with thermal light by passing to higher-order intensity correlations. This idea was realized recently [13] and the growth of ghost-imaging visibility with the order of the registered intensity moment was indeed demonstrated in experiment.

However, as it was pointed out in Refs. [12, 14, 17], it is not the visibility of a ghost image that matters but rather its signal-to-noise ratio (SNR). The noise of a ghost image is related to the variance of the intensity moment under measurement and contains both the shot-noise component and the excess noise component, as well as intermediate terms [14]. Theoretical quantum calculation of the noise for ghost imaging with thermal and nonclassical light has been performed in Ref. [14]; in Ref. [15] the noise for ghost imaging with pseudo-thermal light was also measured experimentally. In Ref. [17] the so called "contrast-to-noise ratio" has been theoretically studied for high-order thermal ghost imaging using a classical approach. However, the present work is the first consideration and experimental measurement of SNR for multiphoton ghost imaging with pseudo-thermal light, i.e., ghost imaging based on higher-order intensity moments.

THEORY

There are many ways to generalize ghost imaging in terms of using higher order intensity correlations. First for the sake of simplicity we consider an (n-1)-port Hanbury-Brown and Twiss (HBT) setup depicted in Fig. 1. As in a standard lensless ghost imaging setup, radiation from a thermal source (usually a rotating ground-glass disk illuminated by a laser beam) is split on a beamsplitter (BS_1). One of the two output beams (the reference one) is further split on n-2 beamsplitters and detected in the far-field zone by n-1 spatially resolving detectors at locations $\mathbf{x}_1, \ldots, \mathbf{x}_{n-1}$. The other (signal) beam is sent to a bucket detector (B) with a mask (M)

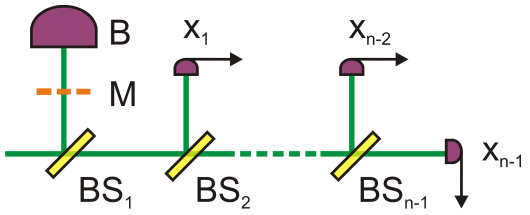

FIG. 1: Schematic of an n-port HBT setup for measuring an n-point n-th order CF.

placed in front of it. Using all n detectors, one measures the intensity correlation function of order n

$$\tilde{G}^{(n)}(\mathbf{x}_1,\ldots,\mathbf{x}_{n-1}) \equiv \langle \prod_{i=1}^{n-1} I(\mathbf{x}_i) \int_{A_s} I(\mathbf{y})T(\mathbf{y})\mathrm{d}\mathbf{y}\rangle, \quad (1)$$

where $I(\mathbf{x}_i)$ and $I(\mathbf{y})$ are instant intensities at corresponding locations measured by (n-1) reference and one signal detectors, respectively. Angle brackets correspond to time-averaging and transmission of the mask is denoted by the function $T(\mathbf{y})$ taking only values 0 or 1. Because the bucket detector collects all signal radiation, integration is implied over its area A_s. Since the bucket detector is supposed to be larger than the mask, integration can be done over the mask area.

Since it is rather complicated to analyze properties of an n-point correlation function (or (n-1)-point ghost image) we focus on a more simple 2-point case where positions of all (n-1) reference detectors coincide: $x_1 = \ldots = x_{n-1} = x$. Eq. (1) then turns into

$$G^{(n)}(\mathbf{x}) \equiv \langle I^{n-1}(\mathbf{x}) \int_{A_s} I(\mathbf{y})T(\mathbf{y})\mathrm{d}\mathbf{y}\rangle. \quad (2)$$

To simplify the calculation, we will consider one-dimensional case and use a very convenient approach of Ref. [15] where a discrete set of modes was introduced. It means that from continuous intensity distributions $I(\mathbf{x})$ we pass to the values of intensities at discrete points $\mathbf{x}_k$, and integration in Eq. (2) is replaced by summation over the modes k' transmitted by the mask, $1 \le k' \le M$:

$$G_k^{(n)} \equiv \langle I_k^{n-1} \sum_{k'=1}^{M} I_{k'}\rangle. \quad (3)$$

Calculation of the intensity correlators from Eq. (3) can be easily performed taking into account that for thermal light

$$\langle I_k^l I_{k'}^m\rangle = \{(l+m)!\,\delta_{kk'} + l!\,m!\,(1-\delta_{kk'})\} I^{l+m}. \quad (4)$$

Here, I is the time-averaged intensity, which is assumed to be uniform over the whole area of the mask, and $\delta_{k,k'}$ is the Kronecker symbol. Hence, for the positions of the reference detector that have counterparts in the signal beam transmitted through the mask, $1 \le k \le M$, the correlation function 3 will take its maximum value,

$$G_{\max}^{(n)} = (n-1)!\,(M+n-1)\,I^n. \quad (5)$$

Otherwise, if k is outside the interval $[1, M]$, the correlation function will take the 'background' value,

$$G_{\mathrm{back}}^{(n)} = (n-1)!\,M\,I^n. \quad (6)$$

The visibility of nth-order ghost imaging can be defined as

$$V^{(n)} \equiv \frac{G_{\max}^{(n)} - G_{\mathrm{back}}^{(n)}}{G_{\max}^{(n)} + G_{\mathrm{back}}^{(n)}}. \quad (7)$$

From Eqs.(5,6), it becomes

$$V^{(n)} = \left(\frac{2M}{n-1} + 1\right)^{-1}, \quad (8)$$

i.e., the visibility grows with the order of the correlation function measured. From Eq.(8), one can see that the visibility decrease due to a large number M of modes in the image can be reduced by passing to a high order n. In the single-mode case, $M = 1$, the values of visibility for different orders are $V^{(2)} = 1/3$, $V^{(3)} = 1/2$, $V^{(4)} = 3/5$,... Note that the results for the maximum and background values of the correlation function, as well as for the visibility, will be the same if quantum-mechanical approach is used in the calculation. However, in the calculation of the noise it is important to use the quantum-mechanical treatment (as, for instance, in Ref. [14], since it is the only way to take into account the shot noise. For this purpose, we will write the expression for the maximum and background correlation functions in the quantum form,

$$G_{\max}^{(n)} \equiv \langle (a_1^\dagger)^{n-1} \sum_{k=1}^{M} a_k^\dagger a_k\ a_1^{n-1}\rangle,$$
$$G_{\mathrm{back}}^{(n)} \equiv \langle (a_0^\dagger)^{n-1} \sum_{k=1}^{M} a_k^\dagger a_k\ a_0^{n-1}\rangle. \quad (9)$$

Here, angular brackets denote averaging over the thermal state of $M+1$ modes whose photon creation and annihilation operators are $a_k^\dagger, a_k$, $k = 0, 1, \ldots M$. The mode $k = 0$ is the only one considered outside of the mask.

We will now calculate the signal-to-noise ratio, taking as the signal the difference $S \equiv G_{\max}^{(n)} - G_{\mathrm{back}}^{(n)}$ and as the noise, the standard deviation of this value, which is

$$\Delta S = \sqrt{\mathrm{Var}(G_{\max}^{(n)}) + \mathrm{Var}(G_{\mathrm{back}}^{(n)}) - 2\mathrm{Cov}(G_{\max}^{(n)}, G_{\mathrm{back}}^{(n)})}, \quad (10)$$

where $\mathrm{Var}(G_{\max}^{(n)})$ and $\mathrm{Var}(G_{\mathrm{back}}^{(n)})$ are variances of the maximum and background correlation functions and $\mathrm{Cov}(G_{\max}^{(n)}, G_{\mathrm{back}}^{(n)})$ is their covariance. The latter has to

be taken into account since $G^{(n)}_{\rm max}, G^{(n)}_{\rm back}$ are not statistically independent.

Calculation of the values entering Eq.(10) is done by passing to normally-ordered correlators using Wick's theorem [16]. For instance, $\mathrm{Var}(G^{(n)}_{\rm back})$ is calculated as

$$\mathrm{Var}(G^{(n)}_{\rm back}) = \\ = \sum_{k=1}^{M}\sum_{k'=1}^{M}\langle (a_0^\dagger)^{n-1}a_k^\dagger a_k a_0^{n-1}(a_0^\dagger)^{n-1}a_{k'}^\dagger a_{k'}a_0^{n-1}\rangle \\ - [(n-1)!]^2 M^2 I^{2n}, \quad (11)$$

which yields

$$\mathrm{Var}(G^{(n)}_{\rm back}) = [(n-1)!]^2 I^{2n} \times \\ \left[\sum_{i=0}^{n-1}\frac{(2n-i-2)!I^{-i}}{[(n-i-1)!]^2 i!}M(M+1+I^{-1}) - M^2\right]. \quad (12)$$

Similarly, calculation of $\mathrm{Var}(G^{(n)}_{\rm max})$ and $\mathrm{Cov}(G^{(n)}_{\rm max}, G^{(n)}_{\rm back})$ leads to the following expression for the signal-to-noise ratio:

$$\mathrm{SNR} = (n-1)\left[\sum_{i=0}^{n-1}\frac{(2n-i-2)!I^{-i}}{[(n-i-1)!]^2 i!}\left\{\frac{n^2(2n-i)(2n-i-1)}{(n-i)^2} + \frac{2(M-1)n(2n-i-1)}{n-i} + 2M^2 + \frac{2M-1}{I}\right\} + \right. \\ \left. + \frac{n^2}{I^n} + \frac{2(1-M-n^2)}{I} - (M-1)(M+4n-1) - M^2 - 3n^2\right]^{-\frac{1}{2}}. \quad (13)$$

In the low-intensity limit, this expression becomes

$$\mathrm{SNR}|_{\mathrm{I}\to 0} = \frac{I^{n/2}(n-1)}{2M-1+n^2}. \quad (14)$$

We see that the signal-to-noise ratio grows polynomially with the intensity of light, the growth index being $n/2$. By plotting dependencies (13) for various orders n for single-mode case (Fig. 2), we see that although the growth is faster for higher n, the signal-to-noise ratio saturates at large intensities, and the maximal values of SNR at higher orders are smaller. Indeed, the high-intensity asymptotic values of SNR are

$$\mathrm{SNR}|_{\mathrm{I}\to\infty} = (n-1)[\frac{2(2n-2)!}{[(n-1)!]^2} \times \\ \{(2n-1)(n+M-1)+M^2\} - \\ -2(M-1)(M+2n) - 3n^2 - 1]^{-\frac{1}{2}}, \quad (15)$$

i.e., they decrease at large n. Analogous calculation for the case of SPDC gives the following expression for SNR

$$\mathrm{SNR}_{\rm SPDC} = \frac{\sqrt{m(m+1)}}{\sqrt{1+7m+7m^2+2Mm(3m+2)+2M^2m^2}}, \quad (16)$$

where m is the mean number of photons per mode. In a high-intensity limit

$$\mathrm{SNR}_{\rm SPDC}|_{\mathrm{m}\to\infty} = \frac{1}{\sqrt{7+6M+2M^2}}, \quad (17)$$

which coincides with the result obtained for second-order thermal ghost imaging.

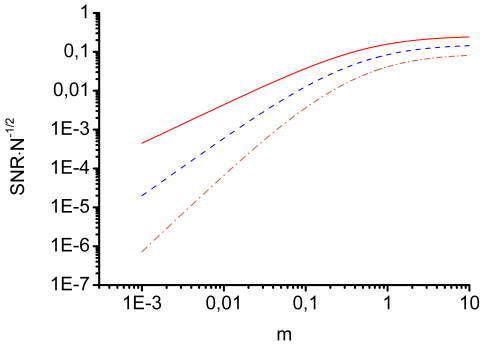

FIG. 2: Normalized SNR dependence on intensity expressed in photons per mode for 2-nd (red solid), 3-rd (blue dashed) and 4-th (orange dot-dashed) order ghost images for single-mode case ($M = 1$).

Fig. 3 shows the dependence of the normalized SNR on the intensity expressed in photons per mode for SPDC and second-order thermal light ghost imaging for single-mode and $M = 10$ cases. As one can see SPDC results in higher SNR values only at low intensities, reaching a maximum value of about 0.27 at intensity of approximately 0.8 photons per mode for the single-mode case. This maximum is just 6% higher that the hight-intensity limit (which is $\frac{1}{\sqrt{15}} \approx 0.26$), so for single-mode case the difference between the maximum SNR obtained with biphotons and the one obtained with thermal light is negligible. For $M = 10$ SPDC has a maximum SNR value of 0.11 at 0.07 photons per mode which is 90% higher

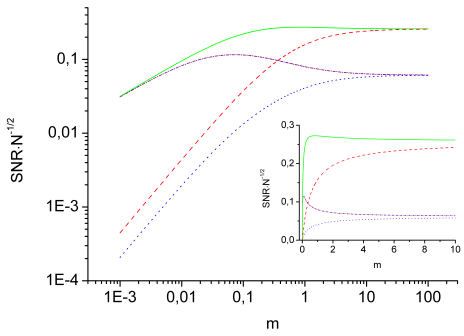

FIG. 3: Normalized SNR dependence on intensity expressed in photons per mode for single-mode SPDC ghost imaging (green solid), thermal light GI (red dashed), SPDC ghost imaging for $M = 10$ (purple dash-dotted) and thermal light GI for $M = 10$ (blue dotted). Given in the inset is the central part plotted in linear scale.

that the high-intensity limit (which is $\frac{1}{\sqrt{267}} \approx 0.06$ for this case).

Experimentally it is more convenient to measure a 2-point correlation function using a 2-port HBT setup (Fig. 4) instead of an n-port setup. Below, we provide a proof of equivalence of the above mentioned setups for strong thermal light (which is the case of consideration) in terms of measuring a 2-point n-th order intensity CF. In quantum description, an n-point n-th order CF is defined by the following expression

$$G^{(n)}(x_1, x_2, \ldots, x_n) = \left\langle \hat{a}_1^\dagger \hat{a}_2^\dagger \ldots \hat{a}_n^\dagger \hat{a}_1 \hat{a}_2 \ldots \hat{a}_n \right\rangle, \quad (18)$$

where $\hat{a}_i^\dagger$ and $\hat{a}_i$ are the photon creation and annihilation operators at point x_i. If n-1 spatial arguments of the CF coincide $x_1 = x_2 = \ldots = x_{n-1}$, it becomes

$$G^{(n)}(x_1, x_1, \ldots, x_1, x_n) = \left\langle \left(\hat{a}_1^\dagger\right)^{n-1} \hat{a}_n^\dagger \hat{a}_1^{n-1} \hat{a}_n \right\rangle. \quad (19)$$

The coincidence counting rate measured by the setup shown in Fig. 4 corresponds to a different 2-point CF, having the form

$$\tilde{G}^{(n)}(x_1, x_1, \ldots, x_1, x_n) = \left\langle \hat{a}_1^\dagger \hat{a}_1 \hat{a}_1^\dagger \hat{a}_1 \ldots \hat{a}_n^\dagger \hat{a}_n \right\rangle. \quad (20)$$

Using the commutation relations one can represent CF (20) as a series of normally-ordered CFs [16]

$$\tilde{G}^{(n)}(x_1, x_1, \ldots, x_1, x_n) = \sum_{i=2}^{n} C_i G^{(i)}(x_1, \ldots, x_n), \quad (21)$$

with $C_n = 1$. Each CF $G^{(i)}$ contains 2i-2 operators taken at point x_1 and two operators taken at point x_n.

Since for thermal light $G^{(i)}$ scales as the i-th order of intensity, in the high-intensity limit the term with $i = n$ in (21) dominates, and CFs (19) and (20) coincide. In this case, our measurement procedure gives the same as the n-port HBT setup.

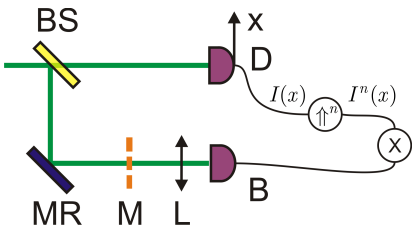

FIG. 4: Schematic of a 2-port HBT setup for measuring a 2-point n-th order ghost image.

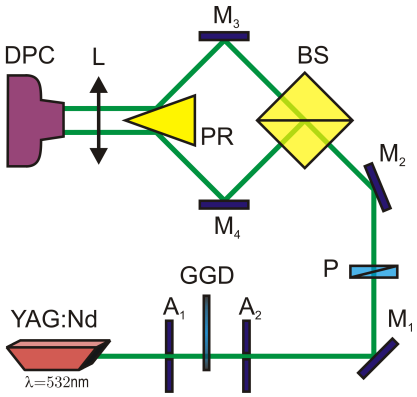

FIG. 5: Experimental setup for measuring n-th order ghost images.

EXPERIMENT

Experimental setup is presented in Fig. 5. As the radiation source, we use a frequency doubled Q-switched Nd:YAG laser with the wavelength 532 nm, pulse duration 5 ns, and the repetition rate of 47 Hz. The laser beam with diameter set by aperture A_1 is projected onto a rotating ground-glass disk GGD to form pseudothermal light. The central part of the speckle field is selected by aperture A_2. Polarizing filter P is introduced to select a linear polarization, thus eliminating any polarization effects introduced by the mirror. Reflecting from mirrors M1 and M2 the beam is divided into two by a nonpolarizing beam-splitter BS. Transmitted (signal) and reflected (reference) beams are reflected by mirrors M3 and M4 respectively. 30-degrees prism PR makes both beams parallel and sends them to a digital photo camera DPC. Lens L is used to image the desired area of the speckle field onto the photo camera's matrix 20.7x13.8 mm (2640x1760 px).

In experiment it is more convenient to use two different parts (signal and reference) of a single CCD camera to capture both signal and reference beams instead of using a CCD and a bucket detector as there is no need to synchronize the latter two. In this case the signal from the bucket detector is obtained by calculating the total signal captured by the reference part of the CCD camera. The idea of using only one CCD camera has been

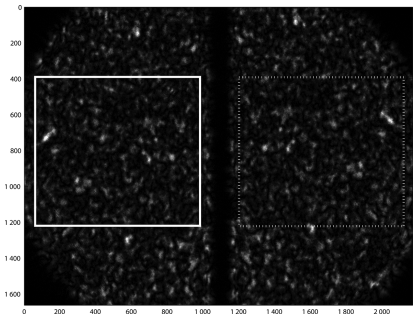

FIG. 6: Single captured frame. The area marked by the solid and dashed white rectangles represent two correlated parts of the speckle field that are selected for ghost image calculation.

recently implemented in experiment [15]. In our case the "software" mask was calculated using a true "physical" realization of the reference beam instead of using only one beam as both signal and reference.

Exposure time was chosen to be 1/50 seconds, so that only one pulse was captured at every frame and the frame rate was about 0.2 fps. Ground glass disk rotation speed was small enough to consider it stationary for the duration of laser pulse and large enough to allow considerable (compared to GGD surface inhomogeneity size) linear displacement between two consequent frames. Thus all the captured frames were time independent and a total of 5000 frames were captured. A typical frame is presented in Fig. 6. The average speckle size was about 30 px (pixels) which correspond to 150μ. By summing the intensities over a desired area (i.e. mask) we obtained the "bucket detector" signal which was correlated with every pixel's signal in the signal arm. Two correlated parts of the signal and reference arms were used for ghost image calculation - they are depicted by solid and dashed white rectangles in Fig. 6.

For clarity we choose a very simple object to image - a single slit represented by a line of 1 px height and variable width. By changing the length of the line one can change the number of modes M. An array of signal values $S(i,j,k,l)$ is calculated as the difference of $G^{(n)}_{\max}(i,j)$ and $G^{(n)}_{\text{back}}(k,l)$. Mean value S of $S(i,j,k,l)$ is then calculated as follows

$$S = \left\langle G^{(n)}_{\max}(i,j) \right\rangle_{\mathcal{M}} - \left\langle G^{(n)}_{\text{back}}(k,l) \right\rangle_{\mathcal{B}},$$

where angle brackets denote averaging that is done over areas $\mathcal{M}$ and $\mathcal{B}$. The first area is a line along the the slit with $j = j_{slit}$ (vertical position of the slit), the latter is a rectangular area of a ghost image outside of the slit. Noise is calculated as the standard deviation of $S(i,j_{slit}) = \left\langle S^{(n)}(i,j_{slit},k,l) \right\rangle_{\mathcal{B}}$.

As one can see from Fig. 7, SNR (the "clarity" of the slit's ghost image) decreases with the growth of the ghost image order as it is predicted by the theory. For a bigger object (a longer slit) this decrease is even more

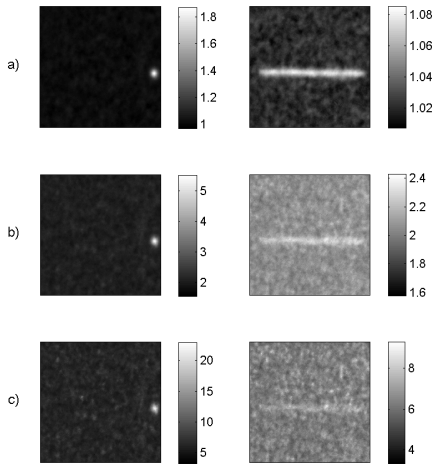

FIG. 7: Ghost images of a short and long one-dimensional single slits for 2-nd (a), 3-rd (b) and 4-th (c) order ghost imaging measured using 5000 frames.

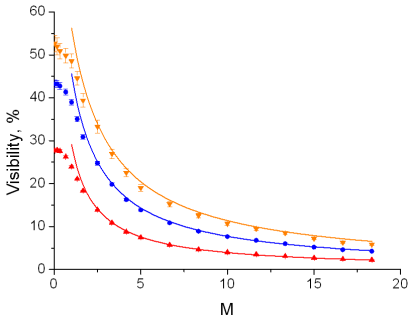

FIG. 8: Visibility dependence on parameter M (number of modes) for the 2-nd (red), the 3-rd (blue) and the 4-th (orange) order ghost imaging of a single slit.

pronounced: the longer slit image has almost drowned in the noise for the case of fourth-order ghost image. By changing the size of the slit in steps one can plot the dependence of visibility and SNR on the size of the mask.

From Fig. 8 it is seen that visibility increases for higher-order ghost images and the values obtained are in a good agreement with the theoretical fit (solid lines). Due to laser power instability over time and GGD inhomogeneity, the fit is made by assuming that the observed values of autocorrelation functions differ from the theoretical values by constant factors $g^{(n)} = F_n n!$ with their values close to unity. As far as the "real" speckle size might be different from the one determined as a FWHM, the parameter M is assumed to be different from a theoretical one by a fixed value S. F_n were independently calculated as mean values of autocorrelation functions of the corresponding order over 5 million pixel areas and make up the following values for second-fourth orders:

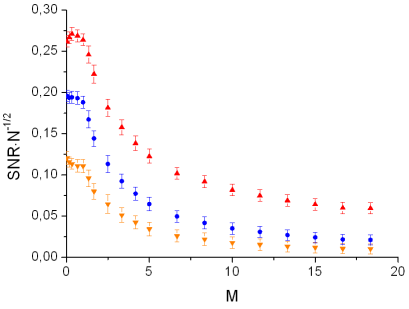

FIG. 9: Normalized SNR dependence on the parameter M (number of modes) for the 2-nd (red), the 3-rd (blue)and the 4-th (orange)order ghost imaging of a single slit.

$F_2 = 0.988$, $F_3 = 0.984$ and $F_4 = 0.997$. The best fit corresponded to $S = 1.19$, which means that the number of modes is determined by speckle width (FWHM) multiplied by S.

In experiment one can only measure sample mean and sample standard deviation, so, in fact, all SNR values are multiplied by a factor of $\sqrt{N}$, where N is the total number of images used to calculate the ghost image. Fig. 9 shows the dependence of the normalized SNR on the number of modes M. One can see that although the visibility does increase with the order, the SNR drops. In order to have the same SNR together with higher visibility values one should increase the number of images N used.

CONCLUSION

We have experimentally performed the 2-nd, the 3-rd and the 4-th order 2-point ghost imaging in pseudothermal light using a 2-port HBT setup and theoretically proved that such measurements are equivalent to those made with 2-, 3- and 4-port setups respectively. We showed that for higher order ghost images defined as in expression (2) there is indeed an increase in imaging visibility and decrease in SNR at the same time. It is found that the second order ghost imaging is optimal for thermal light in the sense of the highest SNR values compared to those in higher orders for a fixed sample size (number of images). Higher visibility values might be obtained using higher order correlations but at the expense of SNR decrease which, in turn, can be compensated by increasing the sampling size.

In the single-mode case thermal light has slightly lower SNR values than SPDC (the difference is less than 6%). In multi-mode case, the difference is larger: ghost imaging with SPDC has a higher SNR maximum compared to thermal light. This result is in agreement with theoretical consideration in [14]. But at high intensities SNR values are the same for both cases at any values of M. From this point of view, if one is interested in best SNR values, thermal light and SPDC give identical result, whereas if one is interested in having the best visibility at a fixed number of images used SPDC has an advantage.

Further research is needed to investigate other cases of ghost imaging experimentally. For instance, recent results [13, 17] suggest that higher SNR can be obtained by exploiting n-th order ghost imaging with symmetrical orders of reference and signal intensities.

This work was supported in part by the RFBR grants # 08-02-00741, # 08-02-00555 and the Program of Leading Scientific Schools Support, # NSh-796.2008.2. I.N.A. acknowledges the support of the 'Dynasty' Foundation.

[1] T. B. Pittman, Y. H. Shih, D. V. Strekalov, and A. V. Sergienko, Phys. Rev. A **52**, R3429-R3432 (1995).
[2] R. Meyers, K. Deacon and Y. Shih, Journal of Modern Optics **54**, Nos. 1617, 23812392 (2007).
[3] M. Zhang, Q. Wei, X. Shen, Y. Liu, H. Liu, J. Cheng, and Sh. Han, Phys. Rev. A **75**, 021803(R) (2007).
[4] B. I. Erkmen and J. H. Shapiro, Phys. Rev. A **78**, 023835 (2008).
[17] R. S. Bennink, S. J. Bentley, R. W. Boyd, Phys. Rev. Lett. **89**, 113601 (2002).
[6] A. Gatti, E. Brambilla, M. Bache, L. A. Lugiato, Phys. Rev. Lett. **93**, 093620 (2004); Phys. Rev. A **70**, 013802 (2004); F. Ferri, D. Magatti, A. Gatti, M. Bache, E. Brambilla, and L. A. Lugiato, Phys. Rev. Lett. 94, 183602 (2005).
[7] G. Scarcelli, A. Valencia, and Y. Shih, Phys. Rev. A 70, 051802(R) (2004); M. DAngelo, A. Valencia, M. H. Rubin, and Y. Shih, Phys. Rev.A 72, 013810 (2005).
[8] D. Zhang, Y. H. Zhai, L. A. Wu, X. H. Chen, Opt. Lett. **30**, 2354 (2005).
[9] X. H. Chen, Q. Liu, K. H. Luo, and L. A. Wu, Opt. Lett. **34**, 695 (2009).
[10] M. Bache, D. Magatti, F. Ferri, A. Gatti, E. Brambilla, L. A. Lugiato, Phys. Rev. A **73**, 053802 (2006).
[11] L. Basano, P. Ottonello, Applied Optics **46**, 6291 (2007).
[12] I. N. Agafonov, M. V. Chekhova, T. S. Iskhakov, L.-A. Wu, Journal of Modern Optics (2009).
[13] X.-H. Chen, I. N. Agafonov, K.-H. Luo, Q. Liu, R. Xian, M. V. Chekhova, and L.-A. Wu, arXiv:0902.3713v1 [quant-ph] (2009).
[14] B. I. Erkmen and J. H. Shapiro, Phys. Rev. A **79**, 023833 (2009).
[15] L. Basano, P. Ottonello, OPTICS EXPRESS **15**, No. 19, 1238617 (2007).
[16] N. N. Bogoliubov and D. V. Shirkov, *Quantum Fields*, Benjamin-Cummings Pub. Co, 1982.
[17] K. W. C. Chan, M. N. O'Sullivan and R. W. Boyd, Opt. Lett. 34, 3343-3345 (2009).